INTERNATIONAL JOURNAL FOR NUMERICAL METHODS IN FLUIDS
Int. J. Numer. Meth. Fluids 2003; **43**:747–768 (DOI: 10.1002/fld.498)

Mesh deformation and modification for time dependent problems

Timothy J. Baker*,†

Mechanical and Aerospace Engineering Department, Princeton University, Princeton, NJ 08544, U.S.A.

SUMMARY

Mesh coarsening and mesh refinement are combined to provide a flexible approach for the adaptation of time dependent problems. When the shape of the domain remains fixed but the computed solution is unsteady (e.g. vortex shedding of laminar flow over a cylinder), successive applications of coarsening and refinement allow the computed solution to be tracked in an efficient manner. The addition of a mesh movement phase extends this technique to handle a domain whose shape is also evolving with time. Copyright © 2003 John Wiley & Sons, Ltd.

KEY WORDS: tetrahedral meshing; mesh movement; adaptation; coarsening; refinement

1. INTRODUCTION

There is a wide and rich variety of interesting problems that are essentially unsteady and which can only be realistically solved if their time dependent nature is fully recognized as part of the finite element computation. This requires a mesh adaptive scheme that is able to follow the evolution of the computed solution and, if necessary, adjust to changes in the shape of the computational domain. For static adaptation (i.e. adaptation to the time dependent changes in the computed solution on a fixed computational domain) mesh coarsening and mesh refinement are the main tools used to achieve the required goal. For dynamic adaptation (i.e. meshes that evolve to follow changes in the shape of the computational domain) it is necessary to augment the mesh coarsening and refinement by a mesh movement algorithm. Details of these components of the adaptation procedure are presented.

Unstructured meshes of triangles in 2D, or tetrahedra in 3D, are particularly well suited to mesh modification since local refinement and/or coarsening can be achieved without the introduction of hanging nodes or other artifices that often plague adaptation schemes for

* Correspondence to: T. J. Baker, Room D302, Department of MAE, Engineering Quadrangle, Princeton University, Princeton, NJ 08544, U.S.A.
† E-mail: baker@tornado.princeton.edu

Contract/grant sponsor: NASA Ames; contract/grant number: NAG-2-1327
Contract/grant sponsor: DOE and NSF; contract/grant number: 00-250 and 00-255

Received 1 April 2002
Revised 26 November 2002

structured meshes. Most of the unstructured adaptive schemes that have been proposed so far exploit h-refinement by directly splitting the elements (i.e. insertion of new points at the midpoints of edges) [1–3]. This approach has the advantage of being relatively straightforward to implement, but can often lead to an excessively large increase in the number of mesh points since each tetrahedron to be fully refined has new points inserted on each of its six edges. The use of Delaunay based techniques for unstructured enrichment provides greater flexibility, allowing new points to be placed wherever and as sparsely as the user deems appropriate.

2. LENGTH DENSITY FUNCTION

The decision whether or not to enrich a particular region of the mesh is based on a comparison between the actual local length scale h (e.g. element width, circum-radius) and the desired length scale specified by a scalar variable ρ called the length density function. Suppose, for example, that the goal is to convert an existing volume mesh into one with a smooth gradation in mesh density throughout the domain and such that the density of the volume mesh near the boundary surface matches the mesh size of the boundary triangulation. The value of the mesh density function at each point on the boundary is computed as the average length of the incident boundary edges [4]. Solving Laplace's equation on the current volume mesh, using the values of the length density function at the boundary as Dirichlet data, will yield appropriate values of ρ at each mesh point. If the value of ρ at any position in the mesh is less than the actual local length scale h then the mesh is refined by the insertion of an extra point followed by a local mesh reconstruction using an incremental Delaunay algorithm. Several possibilities have been considered for selecting the position of point placement (e.g. at element barycentres [4], along edges [5], at element circum-centres [6] or along Voronoï segments [7]). The Voronoï segment method [7, 8] works extremely well in 2D but does not extend readily to 3D. The circum-centre point insertion (CPI) method generates provably good quality meshes in 2D [8, 9]. In 3D the CPI method can generate meshes with good element quality provided care is taken to remove all slivers [10].

For all cases shown in this paper, the actual local length scale h is proportional to the element circum-radius and point insertion is based on the CPI strategy. A element is thus marked for refinement if the circum-radius is too large when compared with the length density function ρ. The local mesh reconstruction exploits a constrained Delaunay algorithm that can be applied to any valid tetrahedral or triangular mesh. Cells to be removed are those whose circumspheres contain the new point subject to the constraint that no boundary face should be removed and that the new point is always visible from the exposed faces of the remaining elements. This particular procedure for inserting a new point is an integral component of the constrained Delaunay method that has been successfully exploited in a number of tetrahedral mesh generators [4, 5, 10].

Mesh coarsening can be achieved by the use of an edge collapse technique whenever the length density function ρ is large compared to the actual mesh length scale h [11].

3. STATIC ADAPTATION

Extra refinement at any mesh position can be achieved by locally reducing the length density function ρ to a value lower than the actual length scale h. If refinement is desired in order

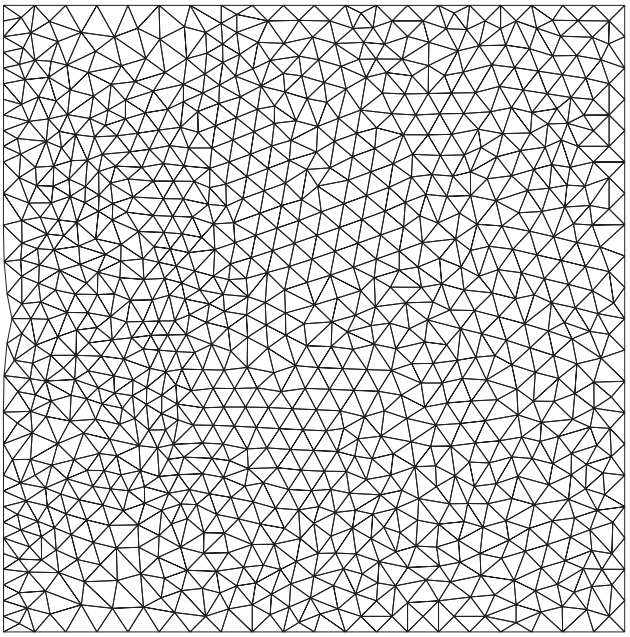

Figure 1. Initial domain and mesh for simulation of crack propagation.

to obtain a more accurate solution, a solution sensor or error estimator e must be constructed to detect regions of rapid change in the computed solution. For the simulation of stress fields in solids the strain energy E can be used as the solution variable to drive adaptation [12]. In particular, a finer mesh is required in regions of high strain energy. The average strain energy $\bar{E}$ is first computed and the standard deviation σ is formed where $\sigma^2 = \overline{E^2} - \bar{E}^2$. Let

$$e = \frac{E - \bar{E} - \lambda\sigma}{\sigma} \tag{1}$$

where λ is a user defined constant. Then

$$\rho_{\text{new}} = \begin{cases} \dfrac{\rho}{1 + \alpha \min(e, 1)}, & E > \bar{E} + \lambda\sigma \\ \rho, & E \leqslant \bar{E} + \lambda\sigma \end{cases} \tag{2}$$

In other words, when the strain energy E exceeds the average plus λ times σ, the length density function ρ is reduced in size. ρ is reduced by at most a factor $1/(1 + \alpha)$ where α is a $O(1)$ user defined constant. Larger values of α create more rapid changes in mesh density while larger values of λ increase the threshold at which adaptation kicks in. This technique has been applied to a variety of problems, including the simulation of crack propagation which involves both static adaptation as well as dynamic adaptation (described in the next section) to adjust the mesh for the deformation that occurs as the crack penetrates the solid. Figure 1 shows the mesh for a rectangular shaped solid that is under lateral tension. An initial defect, modeled by a small depression, is evident on the upper surface. The external tension that is

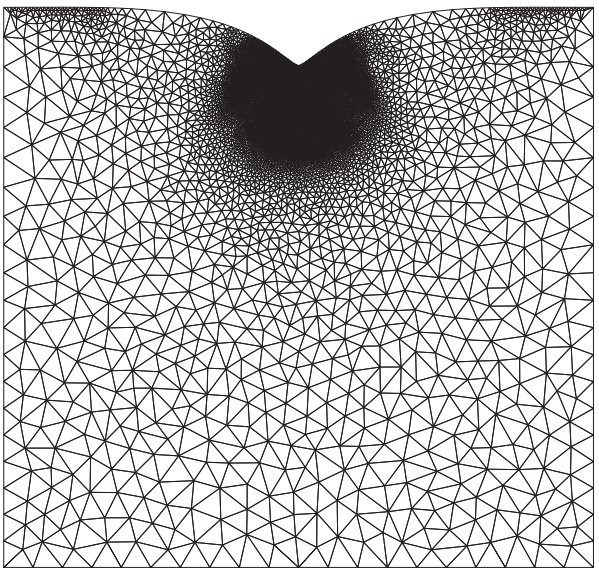

Figure 2. Deformed domain with adaptive refinement near crack tip.

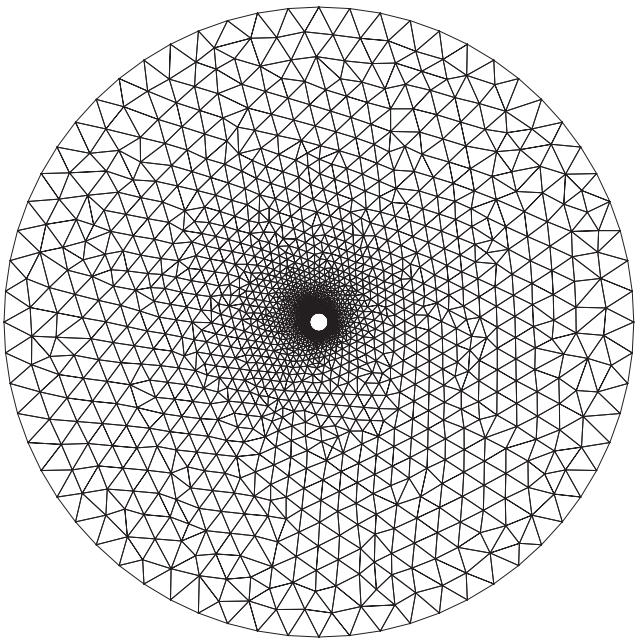

Figure 3. View of complete unadapted mesh at time instant t.

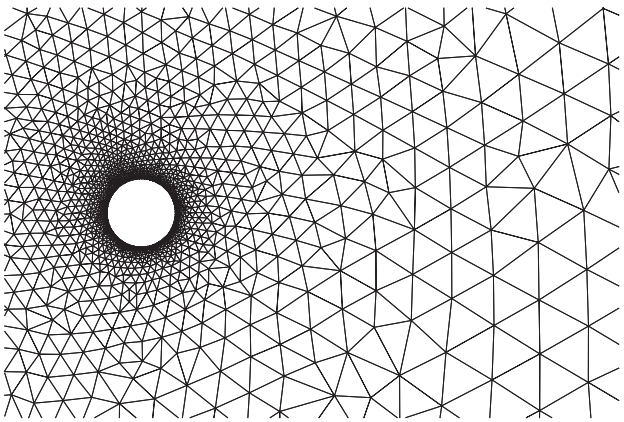

Figure 4. Close up view of the near wake region of the unadapted mesh at time instant t.

applied to the left and right sides of the domain induces a stress field in the solid. This stress field causes material to migrate along the upper surface and away from the region of highest strain energy at the tip of the defect. The resulting deformation in the shape of the upper boundary changes the stress field and increases the strain energy. The defect thus evolves into a crack that steadily penetrates further into the solid. Figure 2 shows the resulting domain and adapted mesh at a particular instant after the crack has formed. The mesh has adapted automatically to the change in domain shape and has become highly enriched in the vicinity of the crack tip in order to resolve the large strain energy values in that region.

An example in which only static adaptation is used can be found in the work of Lin [13]. He presents a computation of incompressible, laminar flow over a cylinder for Reynolds numbers between 50 and 180. Vortices shed from the cylinder are convected downstream so that the flow in the wake region exhibits a periodicity related to the vortex shedding frequency. For this problem the physical property E was taken to be the total pressure. A view of the complete unadapted mesh is shown in Figure 3 and a close up view of the near wake region is presented in Figure 4. Figures 5 and 6 show the corresponding views of the mesh after adaptation to the vorticity field displayed in Figure 7.Note that the mesh density matches the intensity of the vorticity and varies in a reasonably smooth manner between regions of high and low mesh density. Figures 8 and 9 present similar plots of the near field adapted mesh and vorticity distribution at a time that is one half of a period T later. It is evident that the mesh adaptation has successfully tracked the moving vortices, refining the mesh in the new vortex positions and coarsening the part of the mesh that has been vacated by the vortex.

4. DYNAMIC ADAPTATION

Mesh modification for time evolving domains can be carried out by a three stage combination of mesh movement, mesh coarsening and mesh enrichment. One application of this three stage procedure forms one cycle of dynamic adaptation. The extent of domain deformation that can be accommodated during one cycle depends on how far the r-refinement stage can stretch the

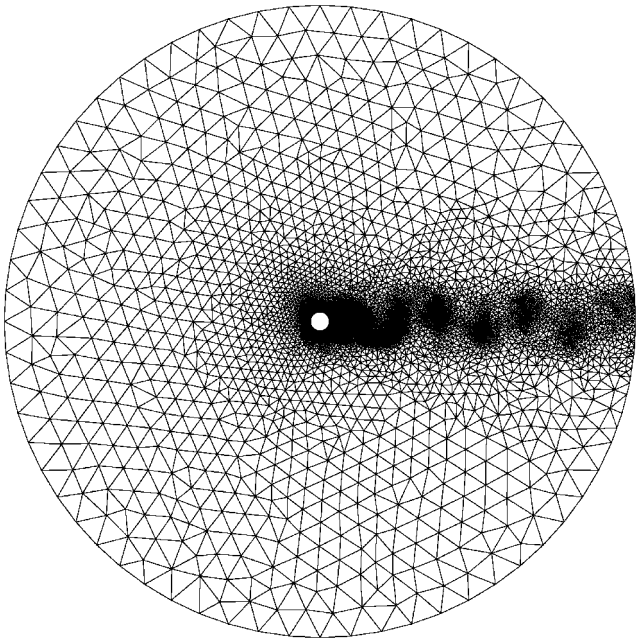

Figure 5. View of complete adapted mesh at time instant t.

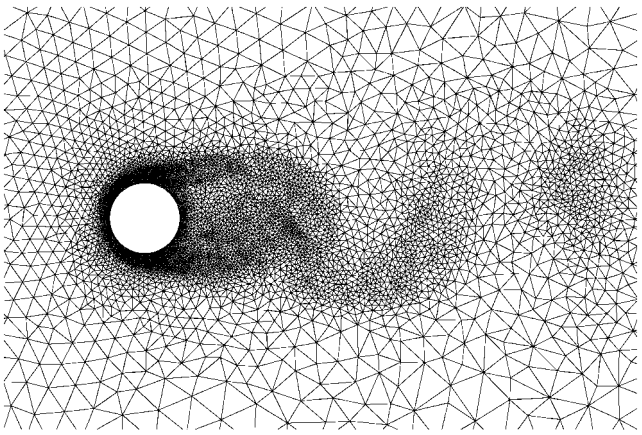

Figure 6. Close up view of the near wake region of the adapted mesh at time instant t.

elements without creating an invalid mesh with negative element volumes. Mesh coarsening is then carried out to remove points associated with elements that have become badly shaped during the r-refinement stage. Finally, mesh enrichment serves to re-create a mesh whose element quality is comparable to that of the original mesh. This modification cycle can be repeated any number of times to obtain a good quality mesh for any homotopic deformation

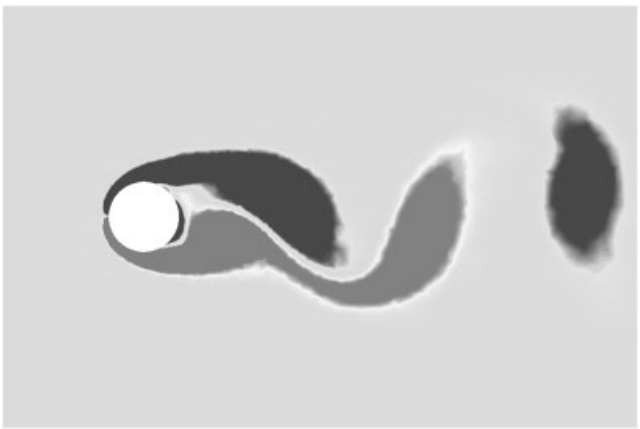

Figure 7. Vorticity distribution in the near wake region at time instant t.

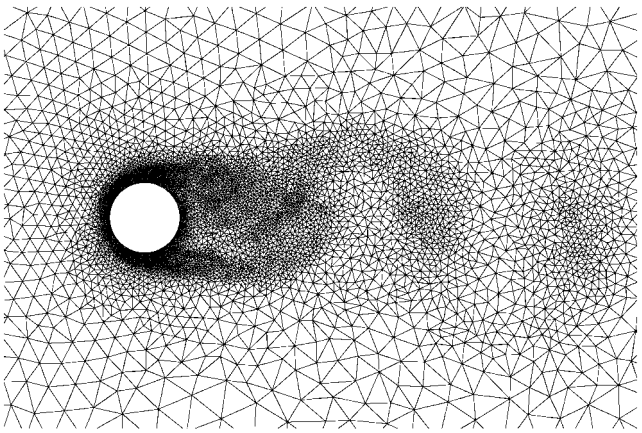

Figure 8. Close up view of the near wake region of the adapted mesh at time $t + \frac{1}{2}T$.

of the boundary. At each stage one is operating on a valid (i.e. conforming, space filling and non-overlapping) mesh which thus avoids the difficulties that are associated with opening up pockets and remeshing.

It is assumed that at a given time level t there exists a valid boundary conforming mesh. During time step Δt the boundary B of the domain is displaced to a new position B', the new boundary position having been determined by the physics of the simulation. At the end of the mesh modification cycle one requires a new mesh at time step $t + \Delta t$ that conforms to the boundary B' and maintains a mesh quality comparable to that of the mesh at time t.

After the mesh movement phase, the mesh quality will be severely degraded, and it is then necessary to identify the badly deformed elements, remove them and insert new mesh points to create a modified mesh that has an acceptable element quality. An appropriate set of badly deformed elements can be identified by exploiting element deformation and shape measures

Figure 9. Vorticity distribution in the near wake region at time instant $t + \frac{1}{2}T$.

[14]. Mesh points, forming this set of elements, are thinned out by a series of edge collapse operations applied to the shortest edge of each such element. The coarsening operation is carried out for all badly deformed elements, including those adjacent to the boundary surface. As a result, there is a selective pruning of points on the boundary surface that are associated with badly shaped surface triangles.

The boundary surface is then refined by inserting new surface points and modifying the incident tetrahedra to create a valid mesh containing the newly inserted boundary surface points. At this stage of the procedure, there is a valid mesh consisting of an acceptable boundary surface triangulation but a volume mesh that still has highly coarsened regions containing overly large tetrahedra. The length density function for all boundary points is then recomputed as the average length of the incident boundary edges. Values of the length density function are distributed to the interior points of the coarsened volume mesh by the Laplacian solver described in Section 2. Finally, enrichment of the volume mesh is carried out by inserting a new point at the circumcentre of any tetrahedron whose circum-radius is too large compared with the local value of the length density function.

5. MESH MOVEMENT

Suppose that the domain D has boundary B at time t and that during time step Δt domain D deforms into D' with boundary B'. One seeks a homeomorphism from D to D' so that a mesh on D is mapped to a valid mesh on D'. Suppose that the point $(x, y, z) \in D$ is mapped to $(x', y', z') \in D'$ and define $\mathbf{u} = (u_1, u_2, u_3)$ where $u_1 = x' - x$, $u_2 = y' - y$ and $u_3 = z' - z$. One may use the mesh on D to solve a suitable elliptic partial differential equation and thus compute the displacement vector $\mathbf{u}$ at all mesh points on D. Adding the computed displacement u_1 to x, u_2 to y and u_3 to z one obtains the new mesh points (x', y', z') on D'. For example, one could solve the Laplace equations $\nabla^2 u_1 = 0$, $\nabla^2 u_2 = 0$, $\nabla^2 u_3 = 0$ subject to the Dirichlet boundary conditions u_1, u_2 and u_3 given on B.

A more robust mesh movement scheme can be constructed by modeling the domain as an elastic solid and solving the equilibrium equations for the stress field [15, 16]. In terms of the displacement vector **u** the strain tensor can be written as

$$\varepsilon_{ij} = \frac{1}{2}\left(\frac{\partial u_i}{\partial x_j} + \frac{\partial u_j}{\partial x_i}\right), \quad i,j = 1,2,3 \tag{3}$$

For an isotropically elastic solid the stress tensor is defined as

$$\sigma_{ij} = \lambda \varepsilon_{kk}\delta_{ij} + 2\mu\varepsilon_{ij}, \quad i,j = 1,2,3 \tag{4}$$

where λ and μ are the Lamé constants, δ_{ij} is the Kronecker delta and the summation convention (viz. $\varepsilon_{kk} = \varepsilon_{11} + \varepsilon_{22} + \varepsilon_{33}$) has been invoked. If there is no distributed body force the stress field satisfies the equation

$$\frac{\partial \sigma_{ij}}{\partial x_i} = 0 \tag{5}$$

Dividing by the shear modulus μ leads to an equation that depends only on the parameter λ/μ. Alternatively, one can introduce Poisson's ratio

$$v = \frac{\lambda}{2(\lambda + \mu)} \tag{6}$$

and consider this to be the user defined parameter.

When mesh coarsening and enrichment is introduced as part of a dynamic adaptation cycle, it is no longer necessary to move the mesh as far as possible during each r-refinement stage.

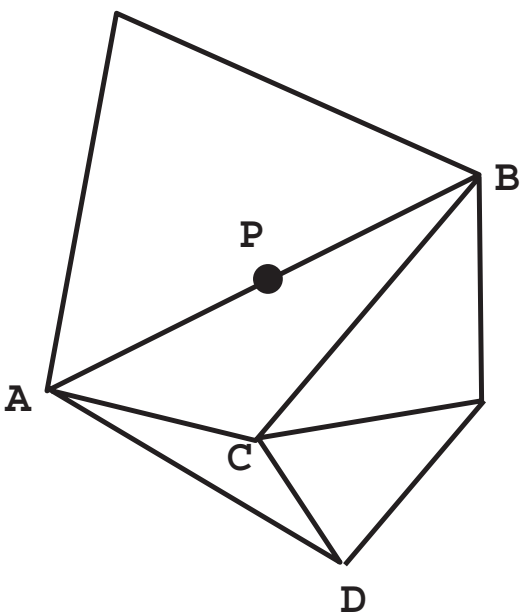

Figure 10. Edge collapse of $\overline{AB}$ onto point P is invalid.

In fact, considerations of computational efficiency favor an r-refinement scheme that permits a smaller degree of mesh deformation if this can be accomplished at a much smaller computational cost than more robust mesh movement methods. In practice, the combined mesh coarsening and enrichment stages account for no more than 20% of the total computation time if the simplest mesh movement scheme is used. For more robust, and thus computationally more expensive, mesh movement schemes the r-refinement stage can consume as much as 95% of the total time.

A particularly simple and cost effective r-refinement scheme is obtained if one approximates Laplace's equation by summing differences of the dependent variable along each edge incident to a mesh point. Introducing a variable diffusivity τ adds only a negligible computational overhead while delaying the onset of mesh breakdown. Define a variable diffusivity by [17]

$$\tau = 1 + \frac{V_{\max} - V_{\min}}{V} \tag{7}$$

where V denotes the volume of an element and $V_{\max}$ and $V_{\min}$ are, respectively, the maximum and minimum element volumes. Let ϕ be the dependent variable and let $\nabla \cdot (\tau \nabla \phi) = 0$ be the equation to be solved. If ϕ_0, respectively ϕ_k, represents the discrete approximation to ϕ at the mesh point P_0, respectively P_k, then the residual at P_0 is given by

$$\nabla \cdot (\tau \nabla \phi)|_0 \approx \frac{1}{S_0} \sum_{k=1}^{m} \sigma_{0k} (\phi_k - \phi_0) \tag{8}$$

where the k summation is over the m edges $\{\overline{P_0 P_k} | k = 1, \ldots, m\}$ incident to the point P_0, the coefficient $\sigma_{0k} = \sum_j \tau_j$ where the j summation is over all the elements incident to the edge $\overline{P_0 P_k}$ and the term $S_0 = \sum_{k=1}^{m} \sigma_{0k}$.

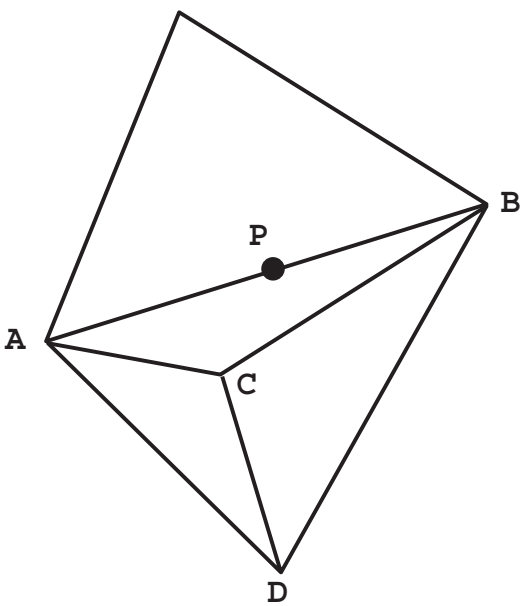

Figure 11. Edge collapse of $\overline{AB}$ onto point P is invalid.

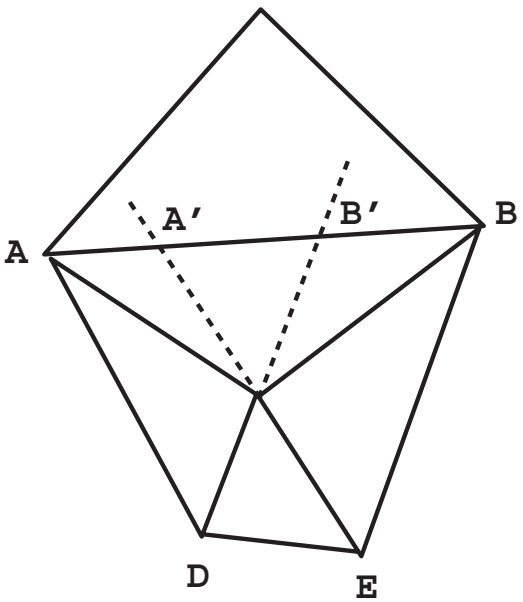

Figure 12. Visibility region is $\overline{A'B'}$.

Using the superscript n to denote the nth iteration, one can write a point Jacobi scheme as

$$\phi_0^{n+1} = \phi_0^n + \frac{\varepsilon}{S_0} \sum_{k=1}^{m} \sigma_{0k}(\phi_k^n - \phi_0^n) \tag{9}$$

where $0 < \varepsilon \leqslant 1$ is a relaxation factor. It is computationally far less expensive than solving the stress equilibrium equations by a finite element method, and the above scheme is the preferred r-refinement method for use in the dynamic adaptation procedure.

6. MESH COARSENING BY EDGE COLLAPSE

The coarsening procedure described in Reference [11] was based on the use of edge collapse in both 2D and 3D. Given edge $\overline{AB}$, the two points A and B would be replaced by a new point P at the mid-point of edge $\overline{AB}$, the edge $\overline{AB}$ and the two triangles (the ring of tetrahedra in 3D) incident to edge $\overline{AB}$ would be removed and the data structure would be updated to correspond to the new mesh that contains one less point. Situations in which this procedure could fail are illustrated for 2D in Figures 10 and 11.

In Figure 10, collapsing edge $\overline{AB}$ onto point P would cause edge $\overline{AD}$ to cross edge $\overline{CD}$ creating an invalid mesh. In the original implementation of the coarsening procedure this edge restriction would result in the edge being left untouched. In this case, however, edge $\overline{AB}$ could be collapsed onto point A leading to a valid mesh. In Figure 11, though, it is clear that there is no point on edge $\overline{AB}$ onto which this edge could be collapsed without creating an invalid mesh. In the original implementation of the method, the smoothing routine that uses edge swapping sufficed to modify the 2D mesh into a state where a further round of

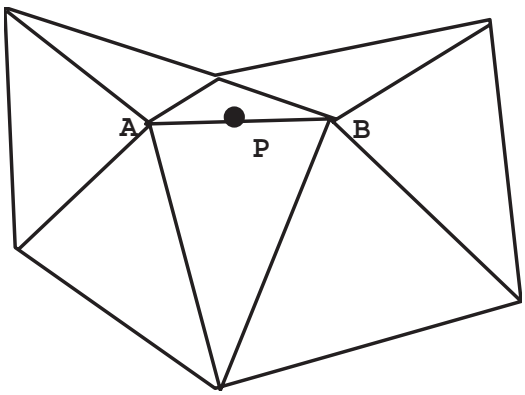

Figure 13. Edge $\overline{AB}$ and associated region D_{AB} .

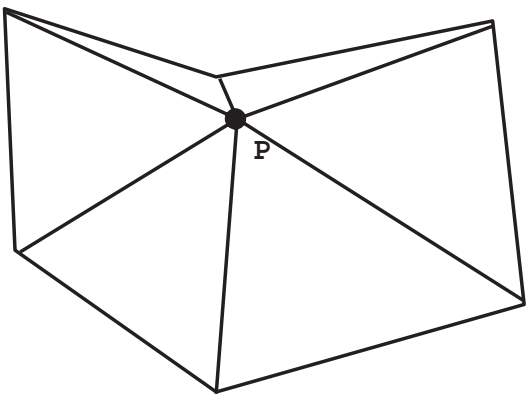

Figure 14. Region D_{AB} after edge collapse onto point P at midpoint of $\overline{AB}$.

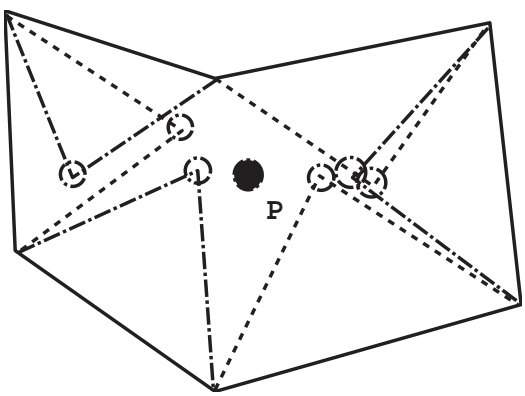

Figure 15. Candidate points P_n' shown by open circles.

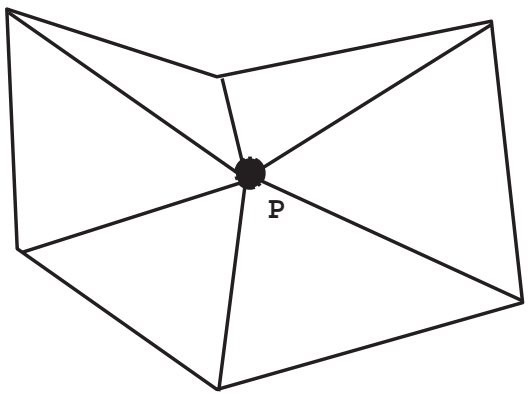

Figure 16. Region D_{AB} after edge collapse onto point P at the modified position.

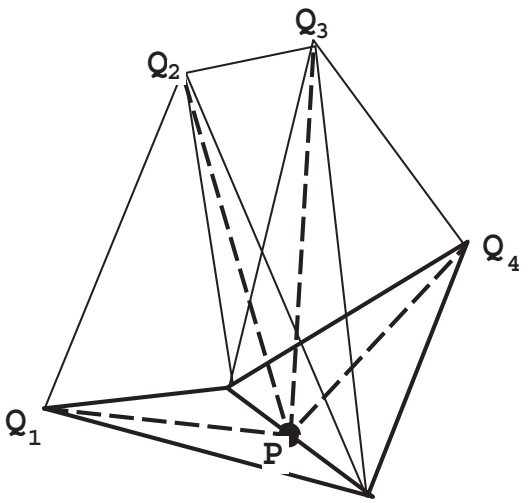

Figure 17. Splitting of boundary faces and tetrahedra.

edge collapse would now permit the removal of edges that were not removed the first time. In 3D there is a richer variety of circumstances in which non-valid tetrahedral combinations can arise when edges are collapsed. Furthermore, the smoothing routines based on a set of edge/face swapping procedures did not always suffice to change the mesh topology to a state where a further round of edge collapse would remove all the remaining edges that had been assigned for treatment.

The edge connectivity of the configuration shown in Figure 11 blocks the application of the collapse procedure for edge $\overline{AB}$. This blocking occurs because vertex C, a vertex associated with one of the triangles incident to edge $\overline{AB}$, has an edge valence of three. This is, of course, the minimum possible edge valence for an internal point in a planar triangulation. An analogous blocking of the collapse procedure occurs in three dimensions if any vertex, other than A or B, in the ring of tetrahedra surrounding edge $\overline{AB}$, has the minimum edge valence

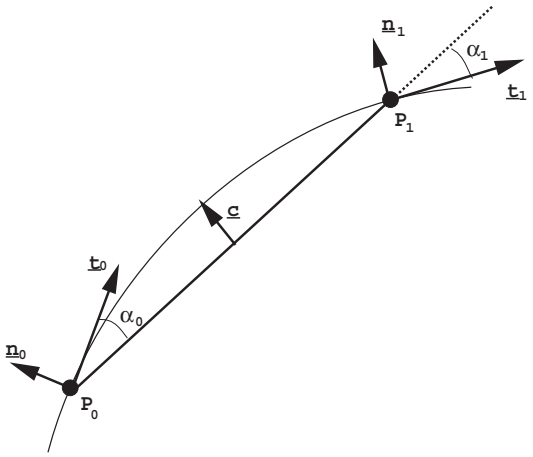

Figure 18. Interpolation of boundary point at edge midpoint as seen in plane Γ.

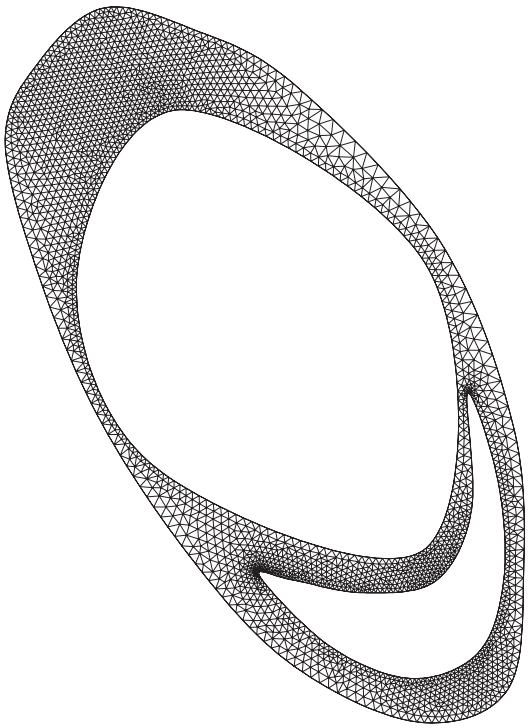

Figure 19. Heart slice at initial position.

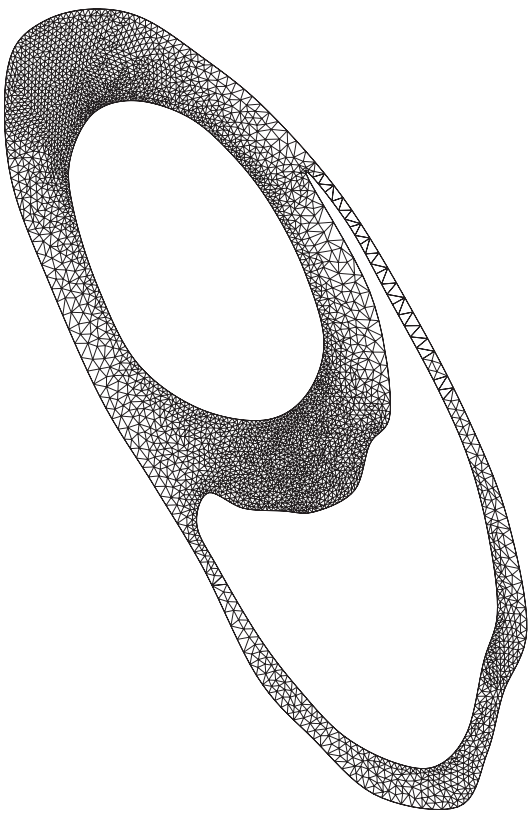

Figure 20. Change in heart slice after one quarter period.

of four. Such cases can be resolved by removing the offending point (point C in Figure 11) and, in the planar case, replacing the three triangles ABC, BDC and DAC by triangle ABD. The equivalent operation in three dimensions is the replacement of four tetrahedra incident to the valence four point by one tetrahedron whose four faces correspond to the faces originally opposite that point.

After removal of all valence four points in the ring of tetrahedra incident to edge $\overline{AB}$, it should be possible to collapse edge $\overline{AB}$ without inverting any neighboring tetrahedra. It is, however, possible that collapse of the edge $\overline{AB}$ is only feasible if the new point P lies in a restricted region of this edge. This is illustrated for the planar case in Figure 12. It is evident that the part $\overline{A'B'}$ of edge $\overline{AB}$ in which P may lie corresponds to the intersection of the regions $\overline{AB'}$ and $\overline{A'B}$ of edge $\overline{AB}$ that are visible from the points D and E respectively.

Placing the new point P at any position on edge $\overline{AB}$ tends to induce a degradation in the quality of the triangles or tetrahedra incident to P (see Figures 13 and 14). The degradation in quality increases with the number of edges collapsed leading to a final coarsened mesh that contains many badly shaped elements. In the planar case, it is possible to recover mesh quality sufficiently well by swapping diagonals of convex pairs of triangles. The mesh enrichment procedure that follows the coarsening and smoothing stage will guarantee a good quality mesh [8, 9].

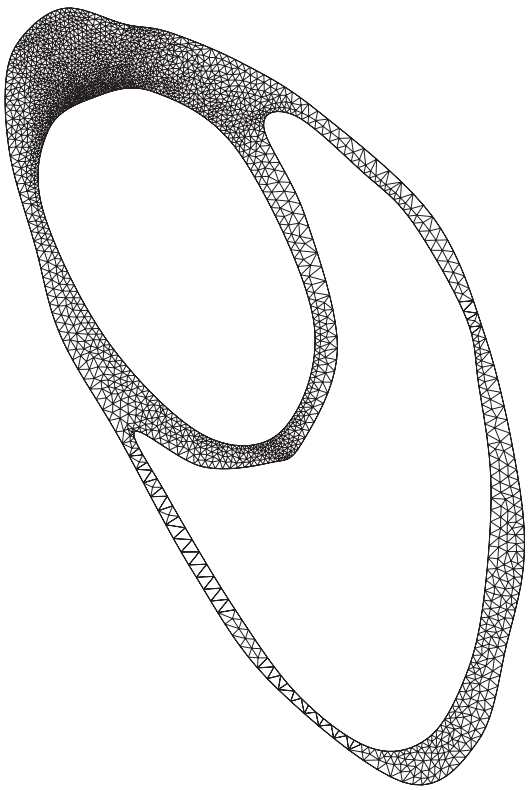

Figure 21. Change in heart slice after one half period.

For tetrahedral meshes, smoothing by edge/face swapping will go a significant way towards the full recovery of a good quality mesh. It is still possible, however, for one or more slivers to remain in the mesh, and the presence of these singular tetrahedra will almost invariably lead to failure of the next mesh movement stage. One way to alleviate this problem is by placing P at a new position off the edge $\overline{AB}$. Define D_{AB} to be the closed region of the meshed domain M occupied by elements that are incident to either point A or point B. The elements contained in D_{AB} all change shape when the edge $\overline{AB}$ is collapsed. Define ∂D_{AB} to be the boundary of D_{AB}. Each edge (face in 3D) in ∂D_{AB} is incident to exactly one triangle (tetrahedron) of D_{AB} and one triangle (tetrahedron) of $M - D_{AB}$. The point P must lie inside D_{AB} and be visible from all edges (faces) of ∂D_{AB}.

In practice, we first associate a candidate position for P with each edge (face) of ∂D_{AB}. Let N be the number of edges (faces) on ∂D_{AB} and denote by $\{P'_n | n = 1, \ldots, N\}$ the N candidate positions of P. The candidate position P'_n for each edge (face) is selected as the vertex of a good quality triangle (tetrahedron) built on the edge (face). In the 2D case, P'_n is chosen to be the vertex that would create an equilateral triangle (shown by the empty circles in Figure 15). In the 3D case, let e be the average edge length of the boundary face and define $h = \sqrt{\frac{2}{3}}e$. The candidate position P'_n is located on the line normal to the face that passes through the face barycentre and at a distance h from the face barycentre. If the boundary face is equilateral

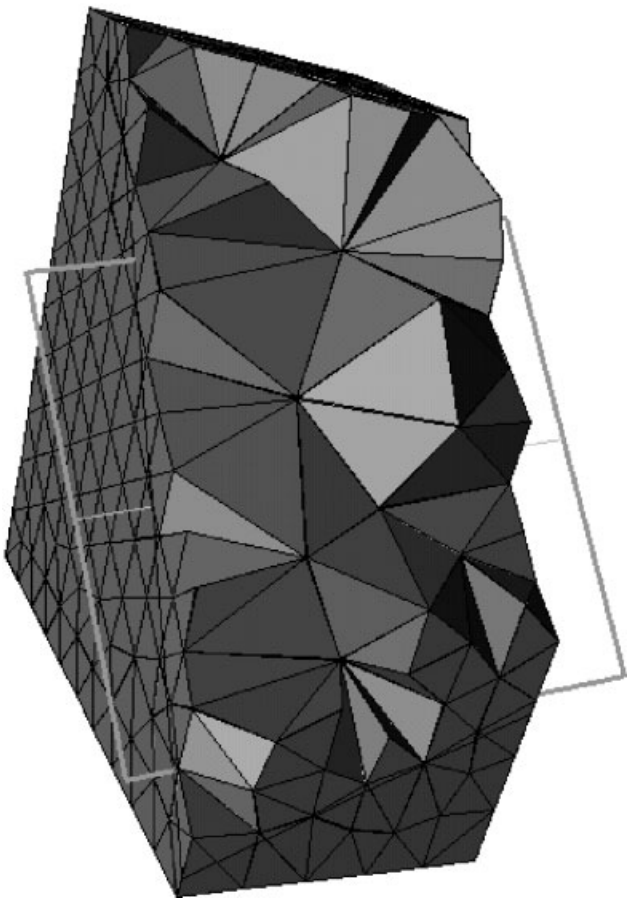

Figure 22. Box surface and cut through volume mesh.

then the candidate position corresponds to the vertex of a regular tetrahedron built on the face. For the general case, when the face is not equilateral, this choice represents a compromise that corresponds to a tetrahedron whose aspect ratio is reasonable.

The new position P is then determined as the average of the N candidate positions [5] (see Figures 15 and 16). In general, the position P will give rise to a collection of good quality triangles (tetrahedra) although it is possible to create an invalid triangulation if the region D_{AB} is non-convex. If the visibility test fails, the point P can be moved closer to the edge $\overline{AB}$ and checked again for visibility.

7. BOUNDARY ENRICHMENT

If the boundary of the computational domain changes shape during the computation, it will be necessary to modify the triangulation of the boundary surface. Coarsening of the boundary triangulation occurs automatically as part of the volume coarsening procedure. It is, however,

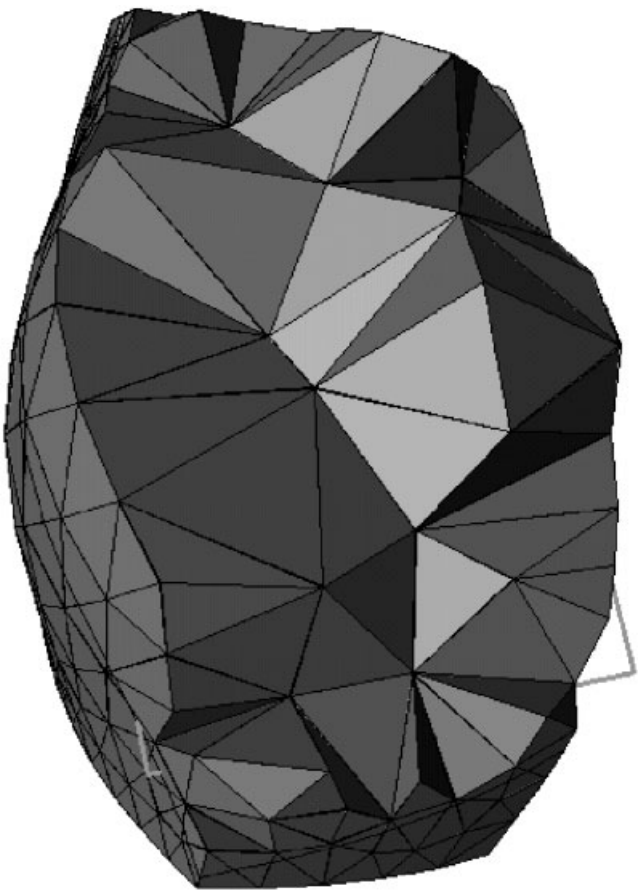

Figure 23. Rounded box surface and cut through volume mesh.

necessary to enrich the surface prior to enrichment of the volume mesh. A boundary face is currently marked for refinement if the maximum edge length is more than twice the minimum edge length. Future developments will seek to enrich the boundary surface based on an assessment of the local curvature.

Each boundary face that has been selected in this way is split by bisecting its longest edge. Inserting a mesh point on a boundary edge will cause both incident boundary faces to be split (see Figure 17). It follows that the state of the boundary triangulation after refinement will depend on the order in which the boundary edges are taken. A list of boundary faces that have been marked for refinement is therefore created and this list is ordered according to triangle aspect ratio (defined as the ratio of circum-radius to in-radius). Starting with the face whose aspect ratio is largest, the longest edge is bisected and the two incident boundary faces are split. Each tetrahedron that is incident to the edge is also split into two new tetrahedra. This procedure is applied in turn to the longest edge of each boundary face that has been marked for refinement. The length density function is recalculated on the boundary and a Laplacian solver is used to distribute the length density function throughout the volume mesh

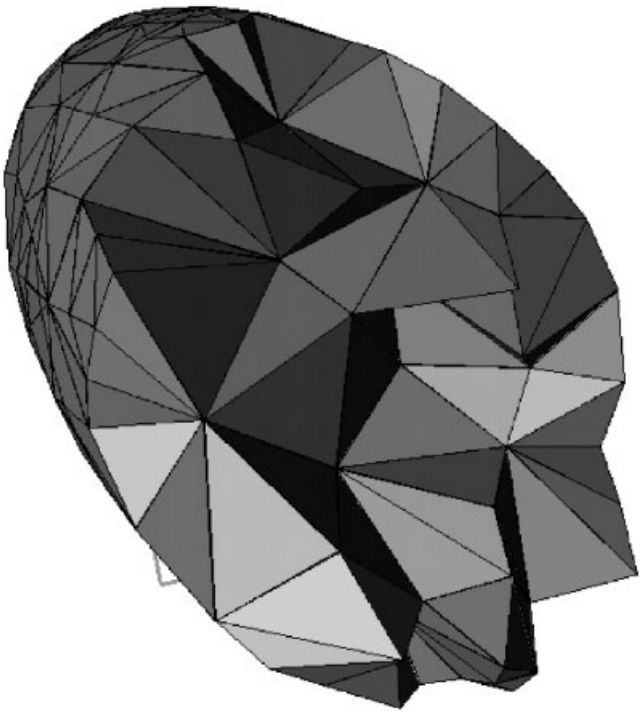

Figure 24. Ellipsoidal surface and cut through volume mesh.

as described in Section 2. Delaunay based tetrahedral refinement is then applied to the volume mesh to complete the enrichment procedure.

It is important to ensure that each new boundary point lies on, or at least close to, the true boundary surface. If this information is not readily accessible then the position can be approximated reasonably well by means of Hermite interpolation. A similar approach has been suggested by Weatherill *et al.* [18] who interpolate new points on boundary faces. The surface enrichment used here only requires the interpolation of new points at the midpoints of boundary edges. The resulting edge and face splitting is applied recursively in a manner that maintains a reasonable level of surface mesh quality. Inserting new boundary points at edge midpoints in a recursive fashion leads to a considerable simplification of the boundary enrichment procedure. There is no need to allow for the multiple splitting patterns that arise when a boundary face is split along one, two or three edges at a time. In addition, Hermite interpolation at the midpoint of an edge assumes a particularly simple form that would not be the case if the new point were placed on the interior of a boundary face.

Let the two endpoints of the boundary edge be P_0 with position vector $\mathbf{x}_0$ and P_1 with position vector $\mathbf{x}_1$, and let the unit normals at these points be $\mathbf{n}_0$ and $\mathbf{n}_1$ respectively. The surface normal at each boundary point is approximated by averaging the normals of the incident boundary faces.

Let $\mathbf{n}$ be the unit normal to the plane Γ in which the new point Q should lie. This plane also contains points P_0 and P_1 and thus the edge joining P_0 to P_1. Fit a cubic polynomial

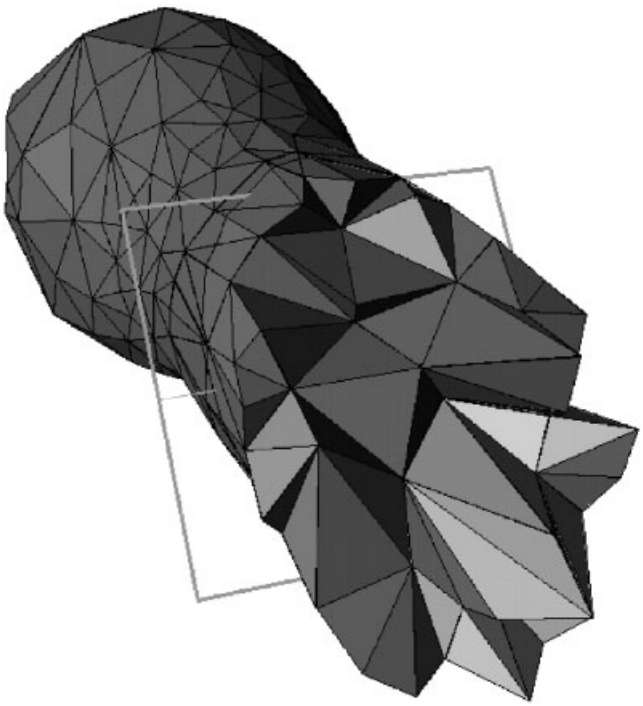

Figure 25. Elongated surface and cut through volume mesh.

lying in the plane Γ through the points P_0 and P_1 whose tangents at P_0 and P_1 are parallel to the corresponding surface tangent planes (see Figure 18). Let $\mathbf{c}$ be the vector from the edge midpoint to the point Q which lies halfway along the interpolating cubic curve. The correction $\mathbf{c}$ thus represents a displacement in the plane Γ that should be added to the coordinates of the edge midpoint in order to obtain an approximation to the true boundary surface.

Let $\mathbf{t}_0$ and $\mathbf{t}_1$ be the tangent vectors lying in the plane Γ. Thus,

$$\mathbf{t}_0 = \frac{\mathbf{n}_0 \times \mathbf{n}}{|\mathbf{n}_0 \times \mathbf{n}|}, \quad \mathbf{t}_1 = \frac{\mathbf{n}_1 \times \mathbf{n}}{|\mathbf{n}_1 \times \mathbf{n}|} \tag{10}$$

Let α_0 be the angle between $\mathbf{t}_0$ and the edge vector $\mathbf{x}_1 - \mathbf{x}_0$. Similarly, define α_1 as the angle between $\mathbf{t}_1$ and $\mathbf{x}_1 - \mathbf{x}_0$ and let $m_0 = \tan\alpha_0$, $m_1 = \tan\alpha_1$, be the imposed slopes of the interpolating curve at each endpoint. For a point lying half way between P_0 and P_1, Hermite interpolation takes a particularly simple form. The displacement is given by

$$\mathbf{c} = \frac{(m_0 - m_1)}{8}\,\mathbf{n} \times (\mathbf{x}_1 - \mathbf{x}_0) \tag{11}$$

In general, the plane Γ, in which the interpolated point should lie, is chosen to be the plane that bisects the dihedral angle between the two boundary faces incident to the edge joining P_0 and P_1. This choice is, however, undesirable at corners or salient edges where the angle between the normals of adjacent faces undergoes a large change. This situation typically

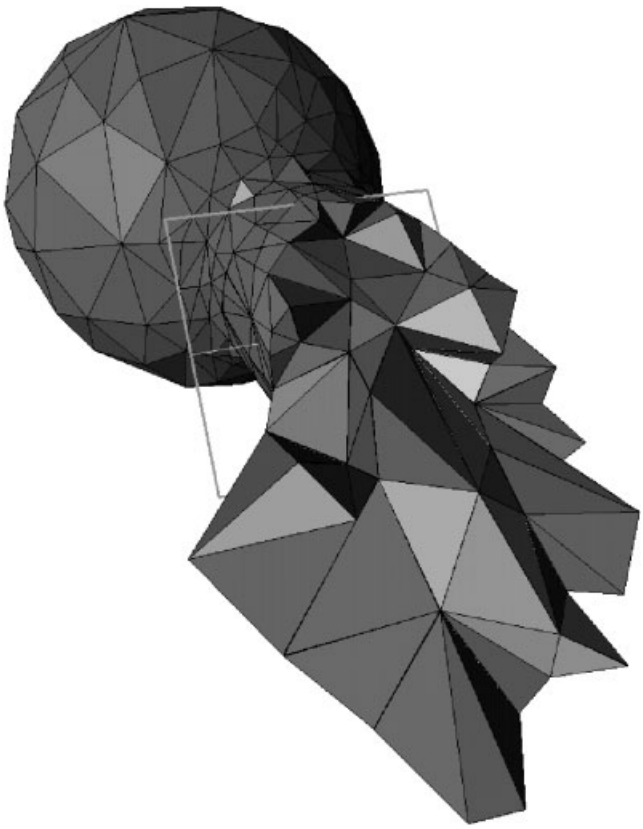

Figure 26. Dumbbell surface and cut through volume mesh.

occurs when two surfaces intersect. It is then preferable to place the new point on one of the two new surfaces so that Γ contains one of the two faces that are incident to the edge joining P_0 to P_1.

8. EXAMPLES

The first example presented in Figures 19–21 shows the result of applying the mesh modification method to a 2-D slice through a heart. The meshed domain consists of heart muscle in the region bounded by the pericardium on the outside and the two ventricles on the inside. During one heart cycle the heart muscle changes shape dramatically and the ventricles alternately contract and expand by considerable amounts. The sequence of figures shows the change in shape during one-half of a cardiac period. The change from Figure 19 to 20 was accomplished in 16 mesh modification cycles with another 16 cycles to go from the state shown in Figure 20 to that shown in Figure 21.

The next five figures show an example of mesh modification for a 3D domain that starts as a box, morphs to a sphere, to an ellipsoid and finally to a dumbbell shape. The complete

sequence takes 45 cycles of the three stage procedure described in this paper. Each of the five snapshots presented in Figures 22–26 was obtained using the vizualization software Medit [19] and shows a cut through the object displaying some of the internal tetrahedra and part of the surface mesh.

ACKNOWLEDGEMENTS

Support for this work has been provided by NASA Ames under grant NAG-2-1327 and by the DOE and NSF under subgrants 00-250 and 00-255 from the University of Illinois.

REFERENCES

1. Baum JD, Löhner R. Numerical simulation of shock interaction with a modern main battlefield tank. *AIAA 22nd Fluid Dynamics, Plasma Dynamics and Lasers Conference*, AIAA Paper 91-1666, Honolulu, HI June 1991.
2. Delanaye M, Essers JA. An accurate finite volume scheme for Euler and Navier–Stokes equations on unstructured adaptive grids. *Proceedings of the 12th AIAA Computational Fluid Dynamics Conference*, AIAA Paper 95-1710-CP, San Diego, CA, June 1995.
3. Biswas R, Thomas SD, Cliff SE. An edge-based solution-adaptive method applied to the AIRPLANE Code. *AIAA 34th Aerospace Sciences Meeting*, AIAA Paper 96-0553, Reno, Nevada, January 1996.
4. Marcum DL, Weatherill NR. Unstructured grid generation using iterative point insertion and local reconnection. *AIAA Journal* 1995; **33**(9):1619–1625.
5. George P, Borouchaki H. *Delaunay Triangulation and Meshing*. Hermes: Paris, 1998.
6. Holmes DG, Snyder DD. The generation of unstructured triangular meshes using Delaunay triangulation. In *Proceedings of the 2nd International Conference on Numerical Grid Generation*, Sengupta *et al*. (eds). Pineridge Press: Swonsea, 1988; 643–652.
7. Rebay S. Efficient unstructured mesh generation by means of Delaunay triangulation and Bowyer-Watson algorithm. *Journal of Computational Physics* 1993; **106**:125–138.
8. Baker TJ. Triangulations, mesh generation and point placement strategies. *Frontiers of Computational Fluid Dynamics*. Caughey DA, Hafez MM (eds). Wiley: New York, 1994; 101–115.
9. Chew P. Guaranteed quality mesh generation for curved surfaces. In *Proceedings of the 9th Symposium on Computational Geometry*. ACM Press: New York, 1993; 274–280.
10. Baker TJ, Vassberg JC. Tetrahedral mesh generation and optimization. *Proceedings of the 6th International Conference on Numerical Grid Generation*. Cross M *et al*. (eds). ISGG, 1998; 337–349.
11. Baker TJ, Cavallo PA. Dynamic adaptation for deforming tetrahedral meshes. *AIAA 14th Computational Fluid Dynamics Conference*, AIAA Paper 99-3253, Norfolk, VA, June 1999.
12. Prevost JH, Baker TJ, Liang J, Suo Z. A finite element method for stress-assisted surface reaction and delayed fracture. *International Journal of Solids and Structures* 2001; **38**:5185–5203.
13. Lin P, Martinelli L, Baker TJ. Two-dimensional implicit time dependent calculations for incompressible flows on adaptive unstructured meshes. *AIAA 15th Computational Fluid Dynamics Conference*, AIAA Paper 2001-2655, Anaheim, CA, June 2001.
14. Baker TJ. Deformation and quality measures for tetrahedral meshes. *Eccomas00*, Barcelona, Spain, Sept. 2000.
15. Johnson AA, Tezduyar TE. Simulation of multiple spheres falling in a liquid-filled tube. *Computer Methods in Applied Mechanics and Engineering* 1996; **134**:351–373.
16. Cavallo PA, Lee RA, Hosangadi A, Dash SM. Dynamic unstructured grid methodology with application to aero/propulsive flowfields. AIAA Paper 97-2310, 1997.
17. Masud A, Hughes TJR. A space-time finite element method for fluid-structure interaction. *SUDAM Report No. 93-3*, Stanford University, Stanford, CA, 1993.
18. Weatherill NP, Marchant MJ, Hassan O, Marcum DL. Grid adaptation using a distribution of sources applied to inviscid compressible flow simulations. *International Journal for Numerical Methods in Fluids* 1994; **19**: 739–764.
19. Frey PJ. Medit: Interactive mesh vizualization software. *INRIA Technical Report RT-0247*, January 2001.

